Numerical investigation on heat transfer of supercritical CO_2 in heated helically coiled tubes

Kaizheng Wang[1], Xiaoxiao Xu*[1],Yangyang Wu[1], Chao Liu[1], Chaobin Dang[2]

1.Key Laboratory of Low-grade Energy Utilization Technologies and Systems, Chongqing University, No. 174 Shazhengjie, Shapingba, Chongqing, 400044, P.R. China

2.Department of Human and Engineered Environmental Studies, The University of Tokyo, 5-1-5 Kashiwanoha, Kashiwa-shi, Chiba 277-8563, Japan

Abstract: Numerical simulation on heat transfer of supercritical CO_2 in heated helically coiled tubes is performed to evaluate the performance of turbulence models in predicting heat transfer of supercritical CO_2 in the helically coiled tube, and to help better understanding the heat transfer mechanism. All turbulence models yield similar tendencies in heat transfer coefficient in the helically coiled tube. The SST (shear-stress transport) model gives the best prediction to the experimental data due to accurate predictions of flow separation under adverse pressure gradients. The parameter of $Gr/\mathrm{Re}^{2.7}$ is incapable of predicting the buoyancy effect onset of supercritical CO_2 in the helically coiled tube. The turbulent Prandtl number has little influence on the calculated heat transfer coefficient.

Key words: numerical simulation, helically coiled tube, supercritical CO_2, heat transfer

* Corresponding author. Tel：+86 023-65112469，Fax：+86 023-65112469
E-mail address: xuxiaoxiao@cqu.edu.cn，(Xu Xiao-xiao).

Nomenclature

a	inner pipe radius [m]
A	surface area [m^2]
b	coil pitch divided by 2π [m]
c_p	specific heat at constant pressure [J/(kg·K)]
C_u, C_ε, C_k	turbulence models' constants
d	tube diameter [m]
D	additional term in the *k*-equation
E	flow energy [W/kg]
f_1, f_2	functions in the dissipation equation
f_μ	damping function
g	acceleration due to gravity[m/s^2]
G	mass flux [$kg/(m^2 \cdot s)$]
Gr	Grashof number
h	heat transfer coefficient [$W/(m^2 \cdot K)$]
k	turbulence kinetic energy [m^2/s^2]
p	pressure [Pa]
P_k	turbulent shear production[W/m^3]
Pr	Prandtl number
q	heat flux [W/m^2]
R	curvature radius [m]
Re	Reynolds number
T	temperature [K]
u	velocity [m/s]

x	Cartesian coordinates [m]
y	normal distance from the inner wall[m]
y^+, y^*	non-dimensional distance from wall
Greek symbols	
β	volume expansion coefficient [K^{-1}]
γ	torsion [b/R]
δ	curvature ratio [a/R]
ε	rate of dissipation of k [m^2/s^3]
θ	global azimuthal angle around the curvature axis [°]
λ	thermal conductivity [W/(m·K)]
μ	dynamic viscosity [Pa·s]
ρ	density [kg/m^3]
$\sigma_k, \sigma_\varepsilon$	turbulent Prandtl number for k and ε
τ	shear stress [N/m^2]
φ	local polar coordinates in the cross-section [°]
Subscripts	
b	bulk fluid
c	circumference of cross-section
cw	node on wall
i	general spatial indices
pc	pseudo-critical
t	turbulent quantity
w	wall

1. Introduction

The heat transfer of supercritical CO_2 in helically coiled tubes appears in power plant technology and cooling systems for heat pump and air-conditioning systems. Supercritical CO_2 is used as an experimental fluid to investigate mechanics of supercritical fluids. Supercritical CO_2 is use as an experimental fluid for two reasons: first, the properties of fluids have similar trends at supercritical pressures. Second, CO_2 reaches the critical point at much lower temperature and pressure compared to that of water, which results in the lower cost of performing experiments [1]. The study of heat transfer of supercritical CO_2 in helically coiled tubes is of great importance in heat exchangers design.

Experimental and numerical studies on the flow and heat transfer of supercritical fluids were performed in straight tubes [2-5]. Dang, *et al*. [6,7] experimentally analyzed the effects of lubricating oil on heat transfer of supercritical CO_2 in horizontal tubes. An experimental investigation on heat transfer of supercritical CO_2 under cooling condition is conducted by Bruch, *et al*. [3]. Jiang, *et al*. [8] carried out experiments on flow and heat transfer of supercritical CO_2 in a porous tube. Experiments on heat transfer of supercritical fluids in micro-tubes were conducted by Withag, *et al*. [9], Oh, *et al*. [10], and Lee, *et al*. [11].

Due to a relatively small tube-diameter used in practice and a relatively high operating pressure for supercritical CO_2, it is hard to measure the practical flow pattern of supercritical fluids directly. Numerical calculation may be the only feasible way to provide such data. Numerical simulation can potentially play a very

important role in improving the understanding of the flow and heat transfer mechanism.

Jiang, *et al*. [12] investigated the heat transfer of supercritical CO_2 in a vertical small tube. The numerical simulation was carried out by using several turbulence models. They found that the low Reynolds number turbulence model proposed by Yang–Shih [13] reproduced the general characteristic occurred in the experiments. Lots of low Reynolds number turbulence models were employed by He, *et al*. [14] to simulate heat transfer of supercritical CO_2 flowing upwards in a vertical tube. They concluded that all of models were able to reproduce some general characteristic to some extent. V2F eddy viscosity turbulence model was used in the numerical computation of heat transfer of supercritical CO_2 in inclined pipes [15]. Research was conducted on the heat transfer of supercritical CO_2 in a vertical small tube with inner diameter of 99.2 μm and the AKN low Reynolds number turbulence model gave the better prediction of the heat transfer than the k-ε realizable turbulence model [16].

Several modes were applied to simulate the heat transfer behavior in straight tubes for supercritical CO_2 and the study showed the JL model [17] gave the best prediction to the heat transfer than other models [18] based on their experimental results [19]. They also concluded that turbulent Prandtl did not have a significant influence on the heat transfer. Cao, *et al*. [20] numerically investigated the laminar heat transfer of supercritical CO_2 in horizontal triangle and circular tubes. The effects of fluid physical properties and buoyancy were analyzed. The heat transfer of

supercritical CO_2 in the tubes was enhanced due to the effect of buoyancy. Numerical studies on heat transfer of supercritical CO_2 were performed by He, *et al.* [21]. They adopted low Reynolds turbulence number of $k-\varepsilon$ model and V2F types. The effect of buoyancy on heat transfer and turbulence production in supercritical fluids could be very significant.

All the above mentioned studies focused on the heat transfer of supercritical fluids in straight tubes. Few studies can be found in open literature on the heat transfer of supercritical fluids in helically coiled tubes. A large amount of experimental and numerical studies of the flow and heat transfer characteristics in the helically coiled tube was concentrated in constant-property fluids, with consideration a variety of situations, such as effects of coiled parameters [22, 23], phase change flow [24, 25], Nanofluids flow [26, 27], ice slurries flow [28], Reynolds number effects [29], Dean number effects [22, 23], and so forth. Jayakumar, *et al*. [23] numerically investigated the local Nusselt number along the length and circumference. Numerical investigation on the heat transfer of water in the helically coiled tube was conducted by Di Liberto, *et al*. [30]. The symmetries of the heat transfer and turbulence were founded. The maximum values were located in the outer side.

Apparently, from the above mentioned researches that focus either on the heat transfer in straight pipes using supercritical fluids, or on the heat transfer in the helically coiled tubes using constant-property fluids. So, it is greatly significant to study the flow and heat transfer characteristics of supercritical CO_2 in the helically

coiled tube.

In this study, the heat transfer of supercritical CO_2 is calculated by some turbulence models. The calculated results are compared with experimental results. The main contents and contributions include the following aspects. First, the performance of turbulence models in predicting the heat transfer coefficient of supercritical CO_2 in helically coiled tubes is evaluated. Second, in order to understand the heat transfer mechanism, we provide the information of the velocity and turbulence kinetic energy. Furthermore, we investigate the effect of the turbulent Prandtl number on the heat transfer of supercritical CO_2 in the helically coiled tube. The paper provides the mechanism of the heat transfer in the helically coiled tube for the design of high-efficiency heat exchanger.

2. Numerical modeling

2.1 Calculation model and Turbulence model

Governing equations for the flow

Continuity:

$$\frac{\partial}{\partial x_i}\left(\rho u_i\right) = 0 \tag{1}$$

Momentum:

$$\frac{\partial}{\partial x_j}\left(\rho u_i u_j\right) = \rho g_i - \frac{\partial p}{\partial x_i} + \frac{\partial}{\partial x_j}\left[\left(\mu + \mu_t\right)\frac{\partial u_i}{\partial x_j}\right] \tag{2}$$

Energy:

$$\frac{\partial}{\partial x_i}\left(u_i(\rho E + p)\right) = \frac{\partial}{\partial x_i}\left(k\frac{\partial T}{\partial x_i} + u_i\tau_{ij}\right) \tag{3}$$

where μ_t is turbulent viscosity which is based on the turbulence model.

The simulation use a number of turbulence models: standard $k-\varepsilon$ model and RNG $k-\varepsilon$ model with enhanced wall treatment, SST $k-\omega$ model [31], AB model [32], LB model [33], LS model [17], YS model [13], AKN model [34] and CHC model [35].

The transport equations for the various models can be expressed in a generic form.

$$\frac{\partial}{\partial x_i}\left[\rho k u_i - \left(\mu + \frac{\mu_t}{\sigma_k}\right)\frac{\partial k}{\partial x_i}\right] = P_k + G_k - \rho\varepsilon + \rho D \tag{3}$$

$$\frac{\partial}{\partial x_i}\left[\rho \varepsilon u_i - \left(\mu + \frac{\mu_t}{\sigma_\varepsilon}\right)\frac{\partial \varepsilon}{\partial x_i}\right] = \left(C_{\varepsilon 1} f_1 P_k + C_{\varepsilon 1} C_{\varepsilon 3} G_k - C_{\varepsilon 2} f_2 \rho\varepsilon\right)\frac{\varepsilon}{k} + \rho E \tag{4}$$

$$\mu_t = \frac{C_\mu f_\mu \rho k^2}{\varepsilon} \tag{5}$$

$$P_k = \mu_t\left(\frac{\partial u_i}{\partial x_j} + \frac{\partial u_j}{\partial x_i}\right)\frac{\partial u_i}{\partial x_j} \tag{6}$$

$$G_k = \beta g_i \frac{\mu_t}{\mathrm{Pr}_t}\frac{\partial T}{\partial x_i}; \qquad \beta = -\frac{1}{\rho}\frac{\partial \rho}{\partial T} \tag{7}$$

The damping functions model and constants are presented in **Table 1**.

2.2 Geometry and mesh model

The mainly geometrical parameters of the helically coiled tube are illustrated in **Fig. 1**. The helically coiled tube can be described by the tube radius (*R*), the coil radius (a) and the coil pitch $(2\pi b)$. In this study, the values of *R*, a, $2\pi b$, are fixed as 141.5 mm, 9 mm, 32 mm , respectively; and the length of the tube is 5500 mm.

The dimensionless torsion and curvature can be defined as:

$$\delta = \frac{a}{R} \tag{8}$$

$$\gamma = \frac{b}{R} \tag{9}$$

Fig. 2 represents the mesh of the simulations which are established in FLUENT preprocessor GAMBIT [36].

2.3 Boundary condition and numerical scheme

The software FLUENT 6.3 is used in the numerical calculation. The conditions are specified that supercritical CO_2 enters the helically coiled tube from the bottom at a temperature of 288 *K* (mass flow inlet boundary condition) and leaves from the top (outflow boundary condition). The supercritical CO_2 is heated by a specified constant wall heat flux.

The couple of velocity and pressure is solved by The SIMPEC algorithm. QUICK is used in the discretization of momentum and energy equations. Turbulence kinetic energy and turbulence dissipation rate equations are adopted second order upwind. When the relative residual of for each governing equation is less than 10^{-5}, the numerical calculation is considered converged.

Supplementary Fig.1 shows thermal conductivities, thermal capacities, densities and dynamic viscosities of supercritical CO_2 at a pressure of p = 8.0 MPa. For the thermodynamic properties, the NIST Standard Reference Database 23 is used. When the pressure is equal to 8.0 MPa, the c_p reached a peak value at the pseudo-critical temperature (T_{pc}) of 307.6 K. The physical properties are used to calculate in FLUENT software by defining a piecewise-linear function of

temperature for the properties of supercritical CO_2.

2.4 Mesh independency

It is important to carry out an independent check of the mesh because mesh quality plays an important role in numerical calculation. The grid number is set to be 781×3076 = 2402356, section×axial. Here, the sectional number represents the total number of grids on one cross section of the tube. Generally, y^+ should be approach to y^+ = 1 to ensure the characteristics near the wall are captured. The dimensionless distance y^+ in the calculation is smaller than 0.8. The mesh is compressed in the axial direction in the radial direction towards the helically coiled wall based on the calculation for each case.

Mesh independency is carried out. Table 2 presents three different numbers of hexahedral meshes. The SST model is applied at the pressure 8.0 MPa, the mass flux 97.8 kg/(s·m^2), the heat flux 9.03 kW/m^2 and the inlet temperature 288 K. The comparisons of calculated T_w are showed in **Fig. 3**. In the **Table 2**, it can be seen that the average relative error between Case-2 and Case-3 is 0.0769%. The grid number which is set to be 2402356 is enough to make the calculated results independent from grids.

3. Results and discussion

Measured data for supercritical CO_2 in helically coiled under heating conditions are presented by Wang, *et al.* [37]. The calculation is performed at the pressure 8.0

MPa, the mass flux 97.8 kg/(s·m^2), the heat flux 9.03 kW/m^2 and the inlet temperature 288 K.

The heat transfer coefficient is calculated by the formula

$$h = q_w / \left(T_w - T_b\right) \tag{10}$$

where the wall temperature T_w is circumferential averaging wall temperature and the T_b at a cross section is defined as

$$T_b = \frac{\int u\rho C_p T \mathrm{d}A}{\int u\rho C_p \mathrm{d}A} \tag{11}$$

where dA is an elemental area of the tube across-section.

3.1 Model comparison and selection

Wen, *et al*. [38] used some turbulence models to simulate the heat transfer features of supercritical water in vertical tube, they found that the SST model was better in predicting heat transfer than $k-\varepsilon$ model. However, Lei, *et al*. [39] concluded that the RNG $k-\varepsilon$ give better prediction than SST model. So the model validation work was required. Numerical investigations on heat transfer of supercritical fluids were conducted by many researchers. They made conclusions that different models performed well at different conditions. Some numerical investigations on heat transfer of supercritical fluids in straight tubes are shown in the **Table 3**

Fig. 4 shows the comparisons of calculated h with the experimental data [37]. Overall, all turbulence models obtain similar tendencies in h along the angle (θ) of the helically coiled tube.

Fig. 4 (a) shows the calculated results of the standard $k-\varepsilon$ model, the SST model and the RNG model. The standard $k-\varepsilon$ model and the RNG $k-\varepsilon$ model overestimate the heat transfer coefficient over the entire angle (θ) range, whereas the SST model simulates well the experimental h, but slightly overestimated the experimental h when $\theta < 720^{o}$.

Fig. 4 (b) shows the three turbulence models cannot predict the experimental h well. The AB model well predicts the measured h over a wild region except in the region of $\theta < 1500^{o}$. The LB model over-predicts experimental h over a wild range of the angle (θ), but underestimates the measured h in the beginning and the end of the helically coiled tube. The LS model overestimates the measured h in whole region.

Fig. 4 (c) shows the calculated results of the AKN model, the YS model and the CHC model. The YS model and the CHC model predict well only in the region of the maximum experimental h and in the beginning of the helically coiled tube, respectively. The AKN model predicts well except $\theta > 1200^{o}$.

From the discussion above, among all the turbulence models in this calculation, the SST model gives the best prediction to the experimental data. The maximum error between the experimental h and the predictions of the SST model is approaching to 10%. In an early study [14], because the non-uniformity of fluid property and buoyancy can lead to extremely distorted flow, the standard $k-\varepsilon$ model with simple wall functions is not appropriate. The literature [44] studies the reasons that the performances of turbulence models are different from one to another.

The different evaluation on turbulence kinetic energy causes different calculation results.

Fig. 5 shows the trends of wall temperature and bulk temperature predicted by SST turbulence model. The SST model reproduces the measured temperature very well whereas slightly underestimates the measured temperature as $\theta > 1600^{o}$. The maximum error between the calculated temperature and experimental temperature is within 2%. In conclusion, the SST model gives the best prediction to the experimental *h*, wall and bulk temperature, indicating that SST model applied in this paper are suitable. Thus, hereinafter, CFD results by SST model are used for further analysis.

3.2 Effects of heat flux

The effects of heat fluxes on the heat transfer performances of supercritical CO_2 in the helically coiled tube are showed in **Fig. 6**. With increasing heat flux, the maximum value decreases. This can be attributed to the radial distribution of properties, especially the influences of thermal conductivity and specific heat. As the increase in heat flux, the heat transfer capacity (c_p) decreases, which results in reducing the influence of c_p on heat transfer . This phenomenon has been discussed by previous studies. Generally speaking, the increase of the heat flux has a significant influence on diminishing heat transfer ability.

Compared with the development of *h* at different mass flux, the profiles of *h* have similar tendency, but some differents on *h* exist at different mass flux. This is

mainly because an increase of mass flux improves the heat transfer ability of supercritical CO_2 due to an increase of turbulent diffusion.

3.3 Flow fields and circumferential distributions of wall temperature and heat transfer coefficient

To better understand the heat transfer mechanism of supercritical CO_2 in the helically coiled tube, the details of some parameters related to heat transfer and flow, such as velocity, turbulence kinetic energy and temperature, are given at the mass flux 97.8 kg/(s·m^2) and the heat flux 9.03 kW/m^2. **Fig. 7** shows the calculated velocity contours at various planes along the length of coil. These contours are displayed from bottom to top along the length of coil (the inlet plane $\theta=0^o$). The selected across sections are oriented in the same way, as shown in **Fig. 1**. Outer side, inner side, bottom and top correspond to $\varphi=0^0$, $\varphi=180^0$, $\varphi=270^0$ and $\varphi=90^0$ respectively.

Without buoyancy, fluid flows faster at the outer side of the helically coiled tube than it does at the inner side due to the effect of centrifugal force (the no-buoyancy pattern in **Fig. 7**). A secondary flow pattern caused by buoyancy is similar to that resulted by centrifugal force. It is interested to note that under the interaction of centrifugal force and buoyancy, the symmetry of flow field is spoiled. In the **Fig. 7**, the maximum velocity region is almost located at the bottom of the cross section ($\varphi=280^0$) at the beginning. This indicates that the effect of buoyancy is dominant over the effect of centrifugal force. With the increase of the bulk

temperature of supercritical CO_2, the maximum velocity region is move towards the top of the tube due to the buoyancy which pushes the heated fluid upward.

Fig. 8 shows the profile of velocity at different angle (θ) along the helically coiled tube. The velocity increases with the increase of angle along the flow direction, and this is because of the flow acceleration caused by the change of density. The velocity varies very rapidly near the wall, and this is attributed to the combined effects of buoyancy force, flow acceleration and centrifugal force.

Fig. 9 and **Fig. 10** show the calculated turbulence kinetic energy contours and profile at different cross sections along the length of the coiled tube. In the **Fig. 9**, the changes of turbulence kinetic energy contours are similar to that of velocity contours. The numerical calculations present the development of the flow field of supercritical CO_2 heated in helically coiled tube. The buoyancy force changes the orientation of the secondary flow and the distribution of velocity and turbulence kinetic energy in the helically coiled tube.

Buoyancy causes the increases of the velocity gradient near the wall and flattening it at the core region of fluid. The effect of acceleration also leads to turbulence to reduce even further at the core region of fluid. The combined effects result in more severe flow laminarization in the core region of fluid as shown in **Fig. 9** and **Fig. 10**, but turbulence kinetic energy near the wall retains a fairly high level.

Though the values of the turbulence kinetic energy at $\theta = 720^o$ where the bulk temperature approaches T_{pc} are slightly larger than the values at $\theta = 270^o$ (**Fig. 10**), the turbulence kinetic energy enhances the heat transfer since turbulence produced

near the wall play an important role in determining the heat transfer capability. The combine effects of high turbulence kinetic energy near wall and the maximum specific heat c_p near the pseudo-critical region result in the wall temperature and the bulk temperature becoming flatter in the vicinity of the critical point which can be seen from **Fig. 5** and the heat transfer coefficient reaches a maximum at about θ = 725^o as seen from **Fig. 4** (a)

The local heat transfer coefficient along the circumference is calculated by the formula

$$h_c = q_w / \left(T_{nw} - T_b\right) \tag{12}$$

where the T_{nw} is a certain node temperature of wall and the T_b is defined as Eq. (11)

The circumferential distributions of heat transfer coefficient (h_c) and wall temperature (T_{nw}) at different axial positions are illustrated in **Fig. 10**. **Fig. 11** shows that the wall temperature close to the top region is higher than other regions; however, the heat transfer coefficients reach a minimum at top region. The effect of buoyancy is dominant over the effect of centrifugal force at the beginning of the helically coiled tube. The buoyancy pushes the heated fluid upward, which results in a maximum wall temperature and a minimum heat transfer coefficient in the top region. The combine effects of buoyancy and centrifugal force make heavy fluid local at φ=280^0. As a result, the heat transfer coefficient at φ=280^0 reach a relatively high level.

3.4 Effects of buoyancy and flow acceleration

Since the buoyancy and flow acceleration significant affect heat transfer, further researches is carried out. The development of heat transfer coefficient and nondimensional value of $Gr/\mathrm{Re}^{2.7}$ calculated by SST model along the angle (θ) is shown in **Fig. 12**. The Grashof number is defined as

$$Gr = g\frac{(\rho_b - \rho_w)a^3}{\rho_b \mu_b^2} \tag{13}$$

where density ρ_b and dynamic viscosity μ_b are based on T_b, density ρ_w is based on T_w, the T_w is peripheral averaging wall temperature.

Full model indicates that the properties in the calculation vary as normal (full model). **Fig. 12** also shows the results calculated by SST model using constant density while other properties vary as normal (ρ=*const*). In this simulation, the density is fixed at constant value based on the fluid temperature of inlet. When ρ is equal to a constant, the influences of buoyancy and flow acceleration caused by the variation of density does not exist.

The heat transfer coefficient of no-gravity flow (no-gravity) is lower than that of the full model, which suggests that the buoyancy force caused by the gravity with density variation makes an enhancement in heat transfer. The heat transfer coefficient calculated by using constant density while other properties vary as normal is higher over a wild range of the angle (θ). The results showed in **Fig. 12** clearly indicate that the change of densities play a significant role in the decrease of heat transfer due to the flow acceleration.

The term $Gr/Re^{2.7}$ proposed by Jackson, *et al*. [45] represents the ratio of

buoyancy to inertia forces. Where, the Grashof Number represents the natural convection of fluid, and the Reynolds Number represents the forced convection of fluid. The term $Gr/Re^{2.7}$ is always used to represent the effect of buoyancy. The criterion for the buoyancy effect is suggested to be greater than 10^{-5}. Buoyancy effect cannot neglect when $Gr/Re^{2.7} > 10^{-5}$. **Fig. 12** shows that the effect of buoyancy increases gradually with the function of the angle (θ), and reaches the maximum near the pseudo-critical point, and then drops along the helically coiled tube. The value of $Gr/Re^{2.7}$ is far below the criterion of 10^{-5}. However, the effect of buoyancy cannot ignore for the helically coiled tube, because the effect of buoyancy makes a discrepancy between full model and no-gravity flow. Therefore, it is necessary to propose a new criterion for supercritical CO_2 heated in the helically coiled tube.

3.5 The influence of turbulent Prandtl number Pr_t

The turbulent Prandtl number in most of the numerical calculations of supercritical fluids is fixed at 0.9 or 1. This is because of the little information about the effect of property variations. So, to find out what results can be achieved is of great importance by using different Pr_t.

To study the effect of Pr_t on heat transfer, the comparisons of h obtained by using the constant values of 0.85, 0.90, 0.95, and 1.00 for Pr_t are showed in **Fig. 13**. There are no visible differences in heat transfer coefficient calculated by SST model using various Pr_t. **Fig. 13** shows that the effect of Pr_t is ignorable under the conditions based on the experiment. A similar conclusion can be found in [18], they

adopted three different Prandtl numbers and showed that the Pr_t did not have a significant influence on the heat transfer.

5. Conclusion

This paper studies the heat transfer of supercritical CO_2 in the helically coiled tube by using numerical calculation method. We can get the following main conclusion.

1) All turbulence models obtain similar tendencies in h along the angle (θ) of the helically coiled tube. The SST model gives the best prediction to the experimental h, wall and bulk temperature. The maximum error between the experimental data and the predictions of the SST model is within 10%.
2) The results reveal the distribution of flow field. Due to the effects of buoyancy and fluid thermal acceleration, the distributions of velocity and turbulence kinetic energy are greatly different from that of constant-property fluids in the helically coiled tube. The effects of buoyancy and centrifugal force result in a maximum wall temperature and a minimum heat transfer coefficient in the top region of the cross section.
3) The parameter of $Gr/\mathrm{Re}^{2.7}$ proposed by previous literature is incapable of representing the influence of buoyancy for the helically coiled tube.
4) The Pr_t has virtually no effect on the calculated heat transfer coefficient for the conditions based on the experiment.

Acknowledge

The authors gratefully acknowledge National Natural Science Foundation of China (Project No. 51206197), Fundamental Research Funds for the Central Universities (Project No. cdjzr12140032) and Chongqing Natural Science Foundation (Project No. CSTC2011BB6094) for providing the financial support for this study.

Reference

[1] S. Gupta, E. Saltanov, S.J. Mokry, I. Pioro, L. Trevani, D. McGillivray, Developing empirical heat-transfer correlations for supercritical CO_2 flowing in vertical bare tubes, Nuclear Engineering and Design, 261 (2013) 116-131.

[2] J.H. Song, H.Y. Kim, H. Kim, Y.Y. Bae, Heat transfer characteristics of a supercritical fluid flow in a vertical pipe, J. Supercritical Fluids, 44 (2008) 164-171.

[3] A. Bruch, A. Bontemps, S. Colasson, Experimental investigation of heat transfer of supercritical carbon dioxide flowing in a cooled vertical tube, International J. Heat and Mass Transfer, 52 (2009) 2589-2598.

[4] M.J. Schuler, T. Rothenfluh, P.R. von Rohr, Simulation of the thermal field of submerged supercritical water jets at near-critical pressures, J. Supercritical Fluids, 75 (2013) 128-137.

[5] B. Niceno, M. Sharabi, Large eddy simulation of turbulent heat transfer at supercritical pressures, Nuclear Engineering and Design, 261 (2013) 44-55.

[6] C. Dang, K. Hoshika, E. Hihara, Effect of lubricating oil on the flow and

heat-transfer characteristics of supercritical carbon dioxide, International J. Refrigeration, 35 (2012) 1410-1417.

[7] C. Dang, K. Iino, E. Hihara, Effect of PAG-type lubricating oil on heat transfer characteristics of supercritical carbon dioxide cooled inside a small internally grooved tube, International J. Refrigeration, 33 (2010) 558-565.

[8] P.X. Jiang, R.F. Shi, Y.J. Xu, S. He, J.D. Jackson, Experimental investigation of flow resistance and convection heat transfer of CO_2 at supercritical pressures in a vertical porous tube, J. Supercritical Fluids, 38 (2006) 339-346.

[9] J.A.M. Withag, J.L.H.P. Sallevelt, D.W.F. Brilman, E.A. Bramer, G. Brem, Heat transfer characteristics of supercritical water in a tube: Application for 2D and an experimental validation, J. Supercritical Fluids, 70 (2012) 156-170.

[10] H.K. Oh, C.H. Son, New correlation to predict the heat transfer coefficient in-tube cooling of supercritical CO_2 in horizontal macro-tubes, Experimental Thermal and Fluid Science, 34 (2010) 1230-1241.

[11] H.S. Lee, H.J. Kim, J.I. Yoon, K.H. Choi, C.H. Son, The cooling heat transfer characteristics of the supercritical CO_2 in micro-fin tube, Heat and Mass Transfer, 49 (2013) 173-184.

[12] P.X. Jiang, C.R. Zhao, R.F. Shi, Y. Chen, W. Ambrosini, Experimental and numerical study of convection heat transfer of CO_2 at super-critical pressures during cooling in small vertical tube, International J. Heat and Mass Transfer, 52 (2009) 4748-4756.

[13] Z. Yang, T. Shih, New time scale based k-epsilon model for near-wall

turbulence, AIAA J., 31 (1993) 1191-1198.

[14] S. He, W.S. Kim, P.X. Jiang, J.D. Jackson, Simulation of mixed convection heat transfer to carbon dioxide at supercritical pressure, Proceedings of the Institution of Mechanical Engineers Part C-Journal of Mechanical Engineering Science, 218 (2004) 1281-1296.

[15] P. Forooghi, K. Hooman, Numerical study of turbulent convection in inclined pipes with significant buoyancy influence, International J. Heat and Mass Transfer, 61 (2013) 310-322.

[16] P.X. Jiang, B. Liu, C.R. Zhao, F. Luo, Convection heat transfer of supercritical pressure carbon dioxide in a vertical micro tube from transition to turbulent flow regime, International J. Heat and Mass Transfer, 56 (2013) 741-749.

[17] B.E. Launder, B.I. Sharma, Application of the energy-dissipation model of turbulence to the calculation of flow near a spinning disc, Letters in Heat and Mass Transfer, 1 (1974) 131-137.

[18] C. Dang, E. Hihara, In-tube cooling heat transfer of supercritical carbon dioxide. Part 2. Comparison of numerical calculation with different turbulence models, International J. Refrigeration, 27 (2004) 748-760.

[19] C. Dang, E. Hihara, In-tube cooling heat transfer of supercritical carbon dioxide. Part 1. Experimental measurement, International J. Refrigeration, 27 (2004) 736-747.

[20] X.L. Cao, Z.H. Rao, S.M. Liao, Laminar convective heat transfer of supercritical CO_2 in horizontal miniature circular and triangular tubes, Applied

Thermal Engineering, 31 (2011) 2374-2384.

[21] S. He, W.S. Kim, J.D. Jackson, A computational study of convective heat transfer to carbon dioxide at a pressure just above the critical value, Applied Thermal Engineering, 28 (2008) 1662-1675.

[22] Y.M. Ferng, W.C. Lin, C.C. Chieng, Numerically investigated effects of different Dean number and pitch size on flow and heat transfer characteristics in a helically coil-tube heat exchanger, Applied Thermal Engineering, 36 (2012) 378-385.

[23] J.S. Jayakumar, S.M. Mahajani, J.C. Mandal, K.N. Iyer, P.K. Vijayan, CFD analysis of single-phase flows inside helically coiled tubes, Computers & Chemical Engineering, 34 (2010) 430-446.

[24] C.N. Chen, J.T. Han, T.C. Jen, L. Shao, Thermo-chemical characteristics of R134a flow boiling in helically coiled tubes at low mass flux and low pressure, Thermochimica Acta, 512 (2011) 163-169.

[25] A. Owhadi, K.J. Bell, Forced convection boiling inside helically-coiled tubes, International J. Heat and Mass Transfer, 10 (1967) 397-401.

[26] N. Jamshidi, M. Farhadi, K. Sedighi, D.D. Ganji, Optimization of design parameters for nanofluids flowing inside helical coils, International Communications in Heat and Mass Transfer, 39 (2012) 311-317.

[27] F. Akbaridoust, M. Rakhsha, A. Abbassi, M. Saffar-Avval, Experimental and numerical investigation of nanofluid heat transfer in helically coiled tubes at constant wall temperature using dispersion model, International J. Heat and Mass

Transfer, 58 (2013) 480-491.

[28] N. Haruki, A. Horibe, Flow and heat transfer characteristics of ice slurries in a helically-coiled pipe, International J. Refrigeration, 36 (2013) 1285-1293.

[29] I. Di Piazza, M. Ciofalo, Numerical prediction of turbulent flow and heat transfer in helically coiled pipes, International J. Thermal Sciences, 49 (2010) 653-663.

[30] M. Di Liberto, M. Ciofalo, A study of turbulent heat transfer in curved pipes by numerical simulation, International J. Heat and Mass Transfer, 59 (2013) 112-125.

[31] F.R. Menter, Two-equation eddy-viscosity turbulence models for engineering applications, AIAA J., 32 (1994) 1598-1605.

[32] R. Abid, Evaluation of two-equation turbulence models for predicting transitional flows, International J. Engineering Science, 31 (1993) 831-840.

[33] C. Lam, K. Bremhorst, A modified form of the k-epsilon model for predicting wall turbulence, ASME Transactions J. Fluids Engineering, 103 (1981) 456-460.

[34] K. Abe, T. Kondoh, Y. Nagano, A new turbulence model for predicting fluid flow and heat transfer in separating and reattaching flows—I. Flow field calculations, International J. Heat and Mass Transfer, 37 (1994) 139-151.

[35] K. Chang, W. Hsieh, C. Chen, A modified low-Reynolds-number turbulence model applicable to recirculating flow in pipe expansion, J. Fluids Engineering, 117 (1995) 417-423.

[36] GANBIT, User's Guide, GAMBIT 2.2.30, FLUENT Inc., (2005).

[37] S. Wang, W. Zhang, Z. Niu, J. Xu, Mixed convective heat transfer to supercritical carbon dioxide in helically coiled tube, CIESC J. , 64 (2013) 3917-3926.

[38] Q.L. Wen, H.Y. Gu, Numerical simulation of heat transfer deterioration phenomenon in supercritical water through vertical tube, Annals of Nuclear Energy, 37 (2010) 1272-1280.

[39] X. Lei, H. Li, Y. Zhang, W. Zhang, Effect of Buoyancy on the Mechanism of Heat Transfer Deterioration of Supercritical Water in Horizontal Tubes, J. Heat Transfer, 135 (2013) 071703-071703.

[40] S. He, W.S. Kim, J.H. Bae, Assessment of performance of turbulence models in predicting supercritical pressure heat transfer in a vertical tube, International J. Heat and Mass Transfer, 51 (2008) 4659-4675.

[41] F.Y. Yang, K. Wang, T. Liu, Y.Q. Wang, Z.C. Liu, Convection Heat Transfer of CO_2 at Supercritical Pressures in Microtubes, Chemical Engineering & Technology, 36 (2013) 2051-2056.

[42] S. He, P.X. Jiang, Y.J. Xu, R.F. Shi, W.S. Kim, J.D. Jackson, A computational study of convection heat transfer to CO_2 at supercritical pressures in a vertical mini tube, International J. Thermal Sciences, 44 (2005) 521-530.

[43] M. Jaromin, H. Anglart, A numerical study of heat transfer to supercritical water flowing upward in vertical tubes under normal and deteriorated conditions, Nuclear Engineering and Design, 264 (2013) 61-70.

[44] S.H. Kim, Y.I. Kim, Y.Y. Bae, B.H. Cho, Numerical simulation of the vertical upward flow of water in a heated tube at supercritical pressure, in: Proceedings of the 2004 International Congress on Advances in Nuclear Power Plants, ICAPP'04, June 13, 2004 - June 17, 2004, American Nuclear Society, Pittsburgh, PA, United states, 2004, pp. 1527-1534.

[45] J. Jackson, W. Hall, Turbulent forced convection in channels and bundles, Hemisphere Publishing Corporation, New York, 1979, pp. 613-640.

Figure captions

Fig. 1. A helically coiled tube with its main geometrical parameters: a, tube radius; R, coil radius; $2\pi b$, coil pitch; The inner (I) and outer (O) sides of the curved duct are also indicated; φ, local polar coordinates in the cross-section; θ, global azimuthal angle around the curvature axis

Fig. 2 Grid of the helically coiled tube used for the simulations

Fig. 3. Comparisons of calculated T_w at different numbers of hexahedral meshes

Fig. 4. Comparisons of calculated h with the experimental data [37]along the angle (θ) of the helically coiled tube(G = 97.8 kg/(m^2·s); q = 9.03 kW/m^2): (a) $k-\varepsilon$ model ($k-\varepsilon$), RNG-$k-\varepsilon$ model (RNG-$k-\varepsilon$), SST model (SST); (b) AB model (AB), LB model (LB), LS model (LS); (c) YS mode (YS), AKN model (AKN), CHC model (CHC).

Fig. 5. Development of wall temperature and bulk temperature predicted by SST turbulence model (G = 97.8 kg/(m^2·s); q = 9.03 kW/m^2)

Fig. 6. Calculated heat transfer coefficients using SST turbulence model at different heat fluxes: (a) G = 100 kg/(m^2·s); (b) G = 300 kg/(m^2·s)

Fig. 7. Contours of velocity magnitude and secondary velocity vectors for different cross sections along the helically coiled tube

Fig. 8. Radial distributions of velocity magnitude predicted by the SST model

Fig. 9. Turbulence kinetic energy contours for different cross sections along the helically coiled tube

Fig. 10. Radial distributions of turbulence kinetic energy predicted by the SST

model

Fig. 11. Circumferential distributions of wall temperature and heat transfer coefficients at different axial positions (Outer side, inner side, bottom and top correspond to φ=0^0, φ=180^0, φ=270^0 and φ=90^0 respectively): (a) wall temperature; (b) heat transfer coefficients

Fig. 12. Influences of buoyancy and flow acceleration on heat transfer

Fig. 13. Comparison of the heat transfer coefficients predicted by SST model using various constant Pr_t

Figure 1

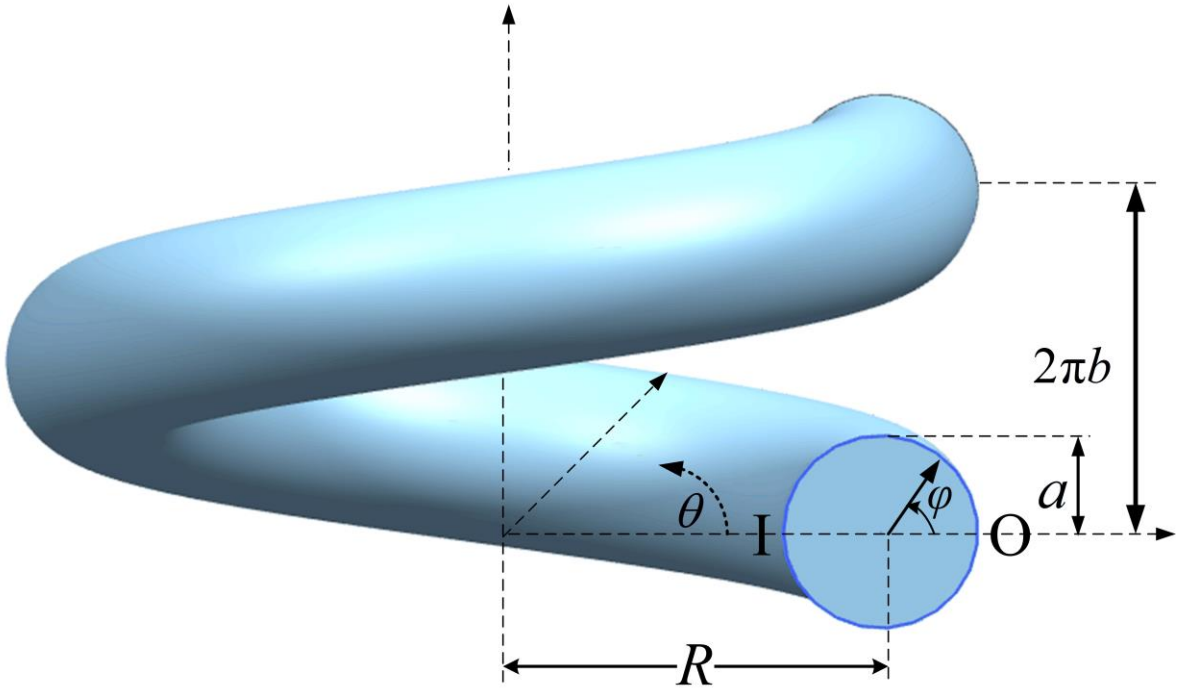

Figure 2

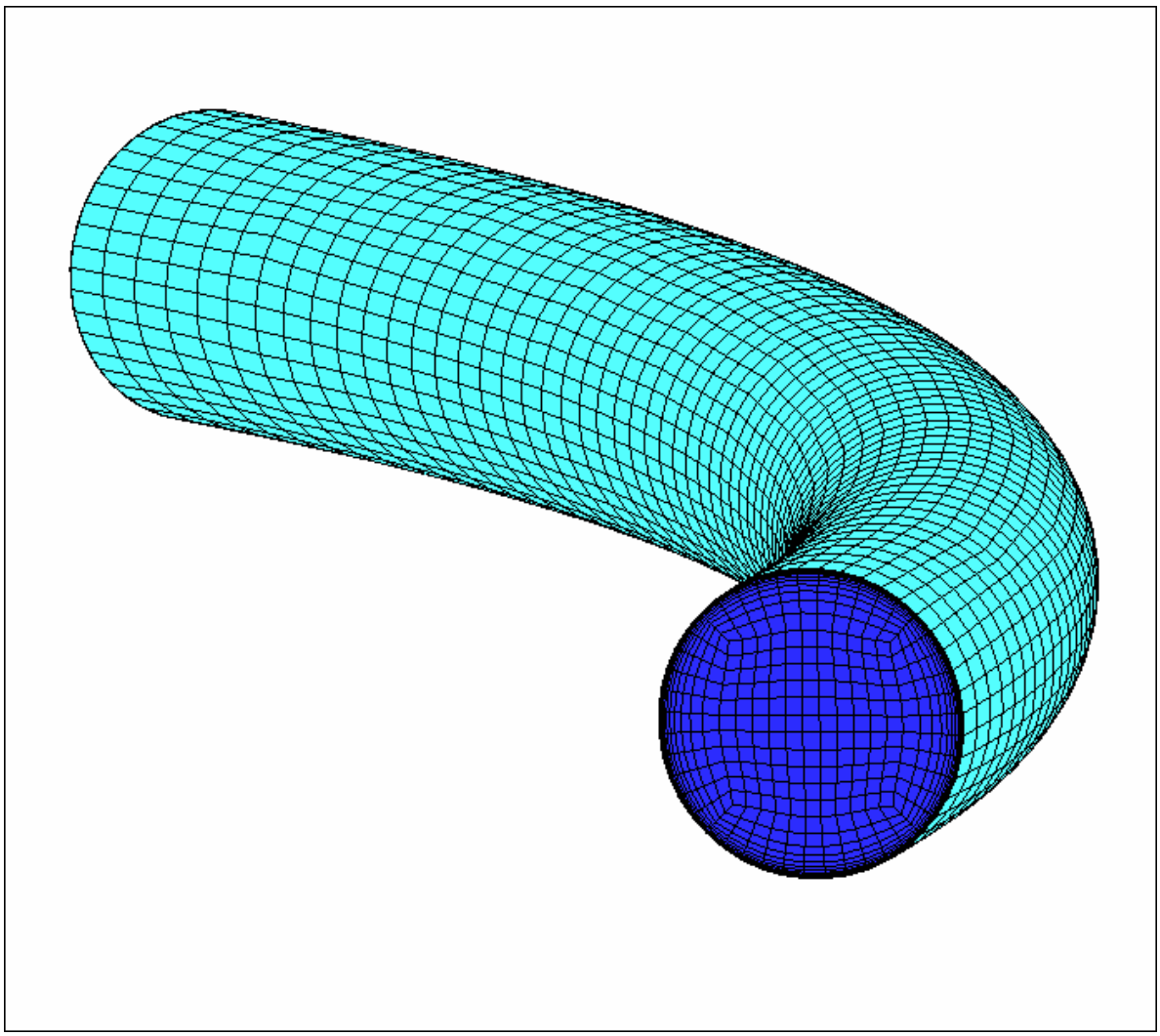

Figure 3

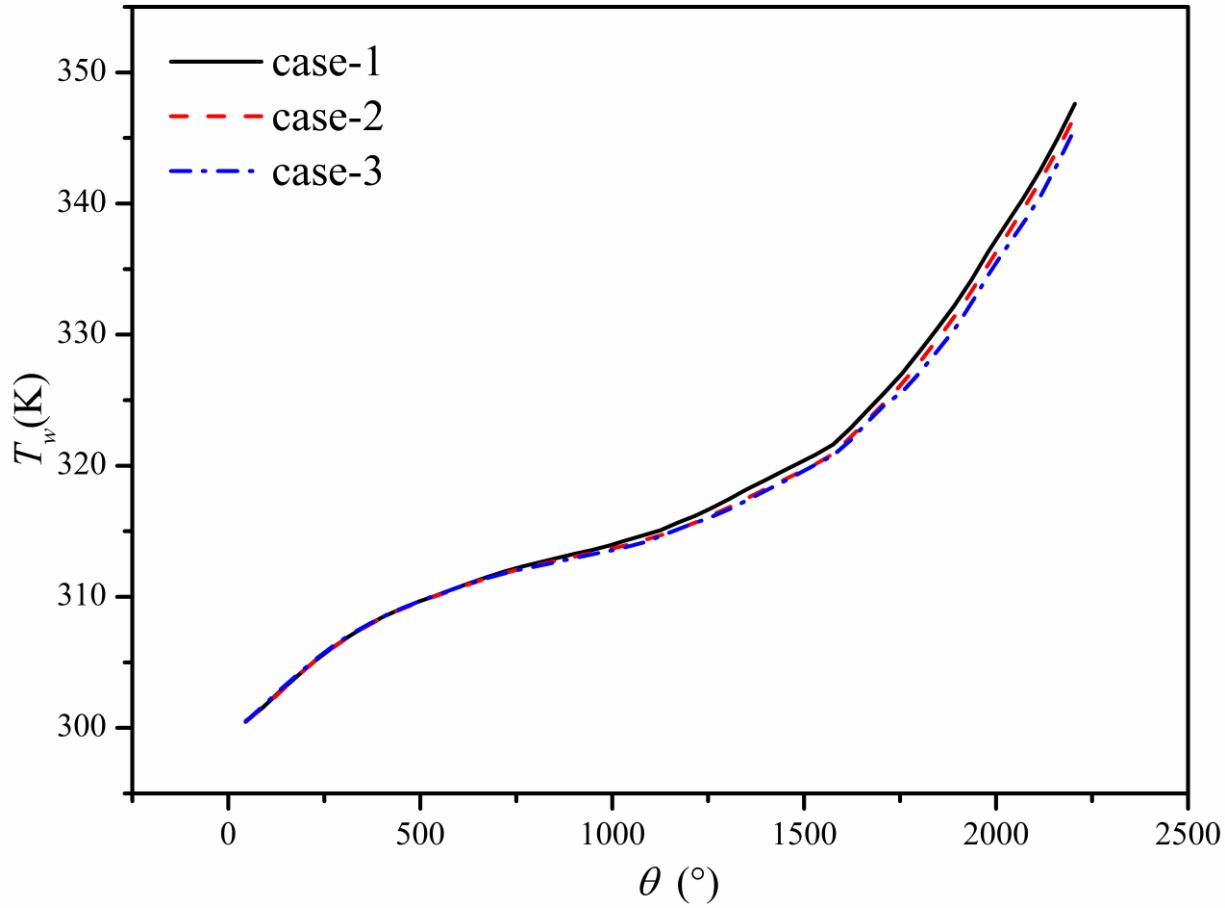
case-1
case-2
case-3
350
340
330
320
310
300
T_w (K)
0
500
1000
1500
2000
2500
θ (°)

Figure 4

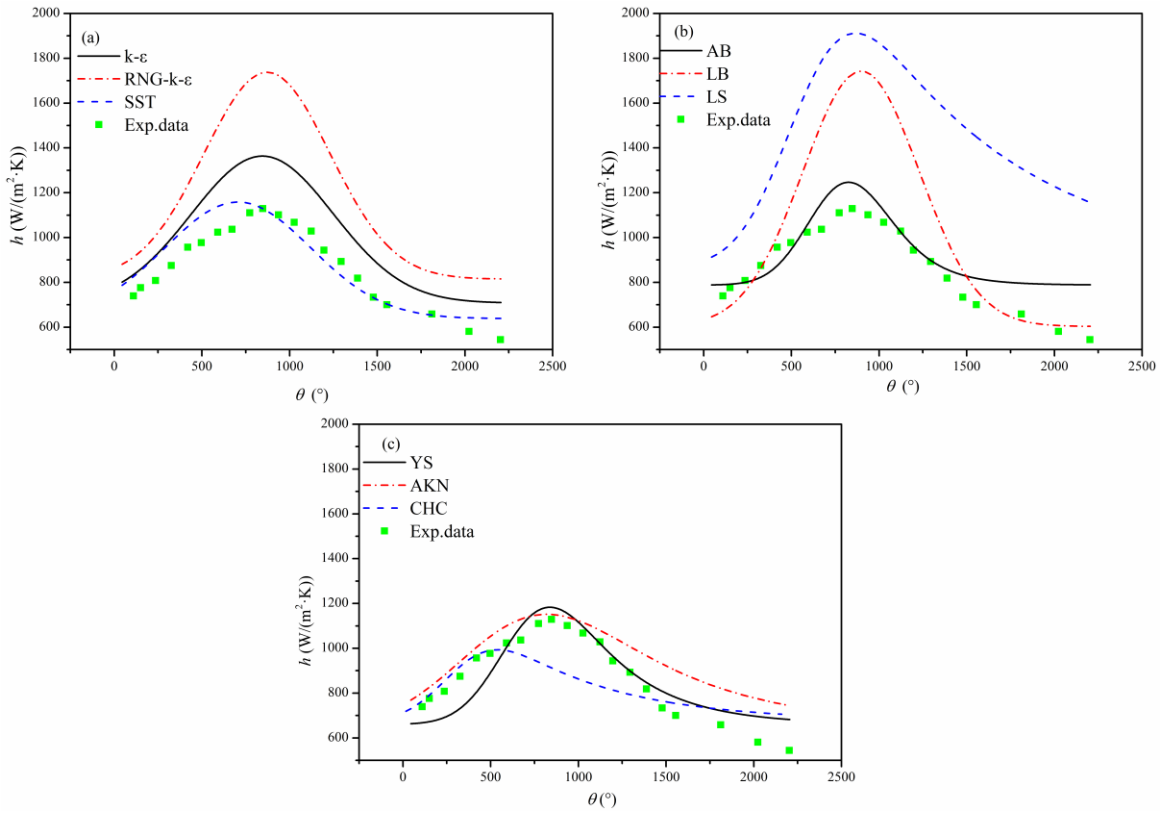
(a)
k-ε
RNG-k-ε
SST
Exp.data
h (W/(m²·K))
θ (°)
(b)
AB
LB
LS
Exp.data
h (W/(m²·K))
θ (°)
(c)
YS
AKN
CHC
Exp.data
h (W/(m²·K))
θ (°)

Figure 5

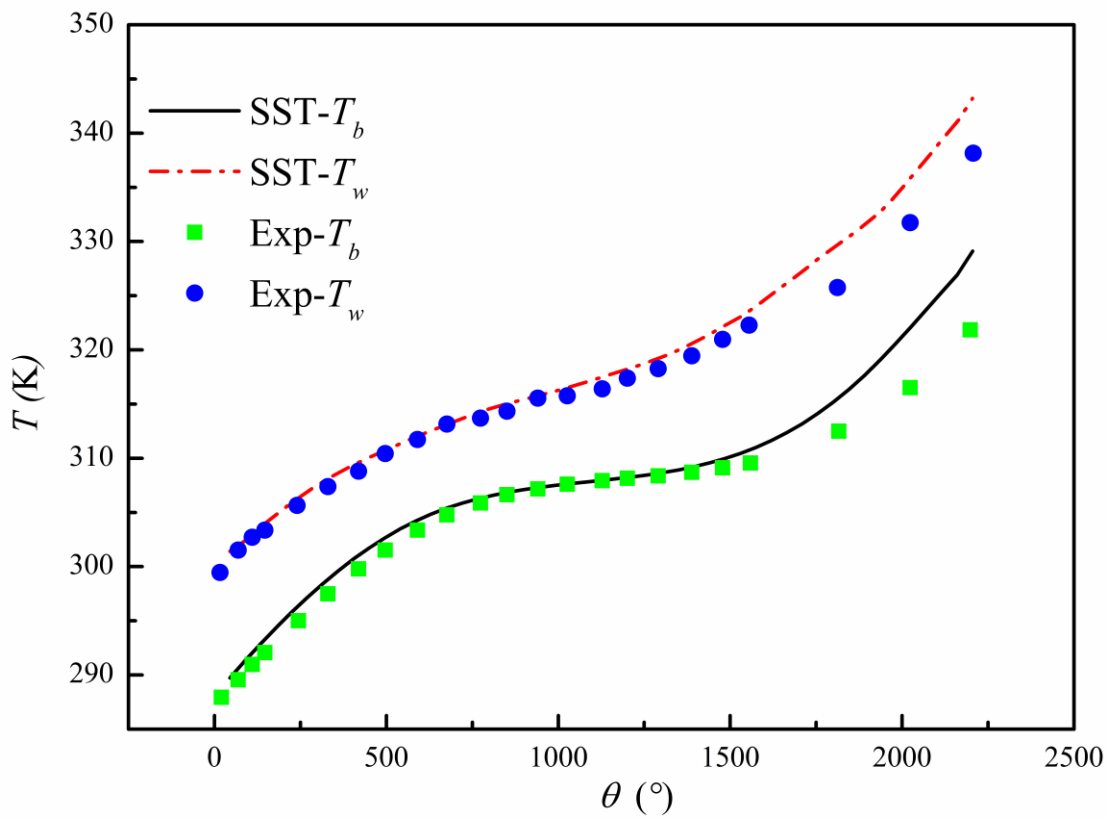
350
340
330
320
310
300
290
T (K)
SST-T_b
SST-T_w
Exp-T_b
Exp-T_w
0
500
1000
1500
2000
2500
θ (°)

Figure 6.

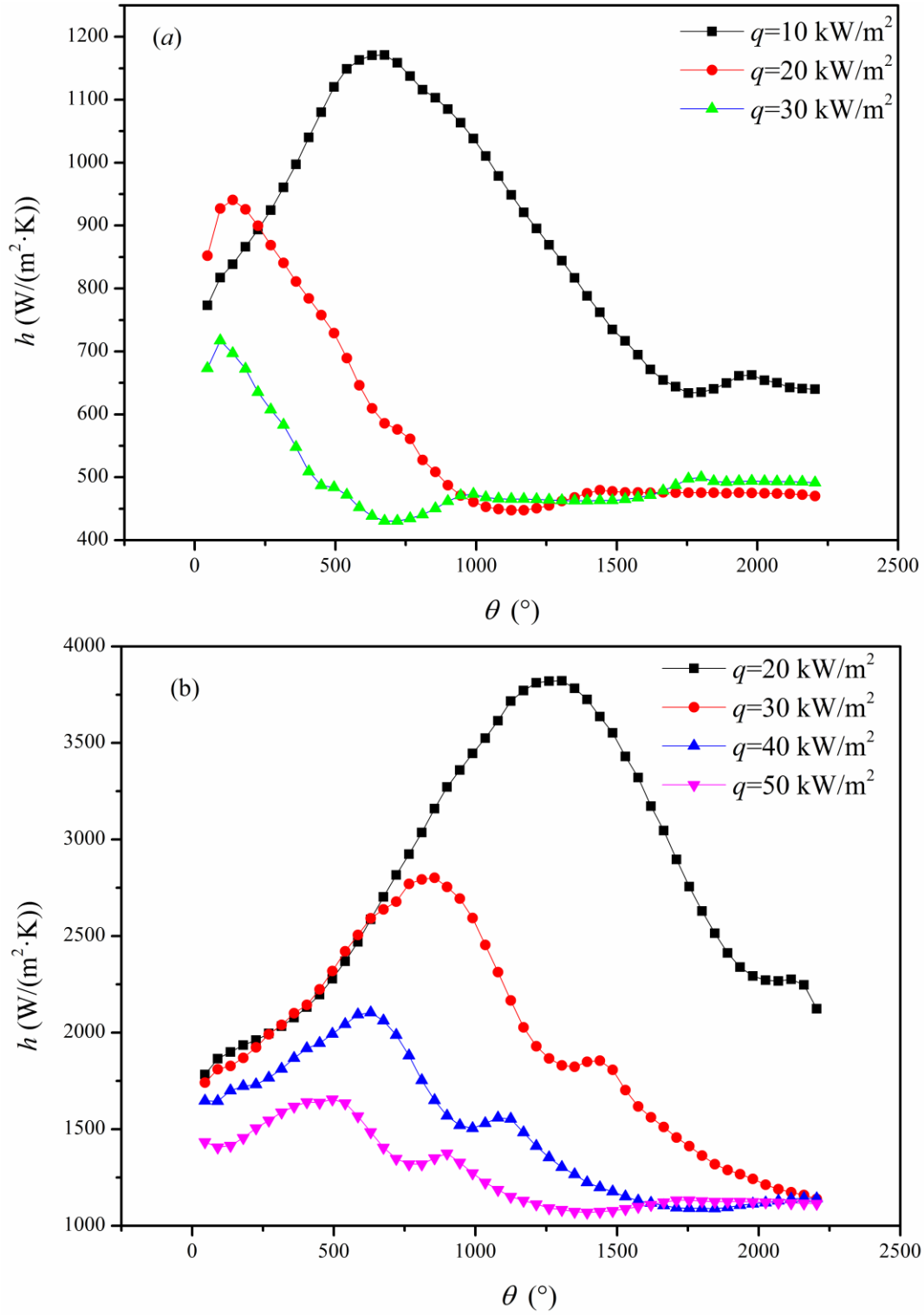
(a)
q=10 kW/m2
q=20 kW/m2
q=30 kW/m2
h (W/(m2·K))
θ (°)
(b)
q=20 kW/m2
q=30 kW/m2
q=40 kW/m2
q=50 kW/m2
h (W/(m2·K))
θ (°)

Figure 7

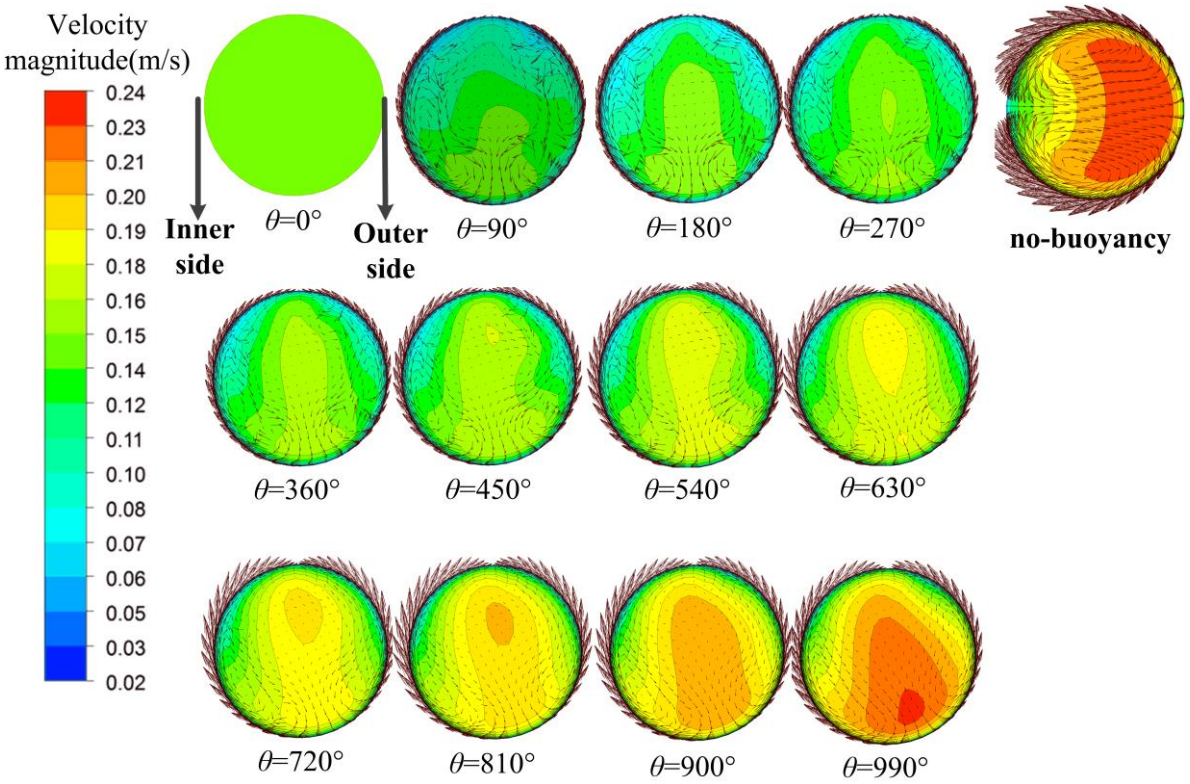
Velocity magnitude(m/s)
0.24
0.23
0.21
0.20
0.19
0.18
0.16
0.15
0.14
0.12
0.11
0.10
0.08
0.07
0.06
0.05
0.03
0.02
Inner side
Outer side
θ=0°
θ=90°
θ=180°
θ=270°
no-buoyancy
θ=360°
θ=450°
θ=540°
θ=630°
θ=720°
θ=810°
θ=900°
θ=990°

Figure 8

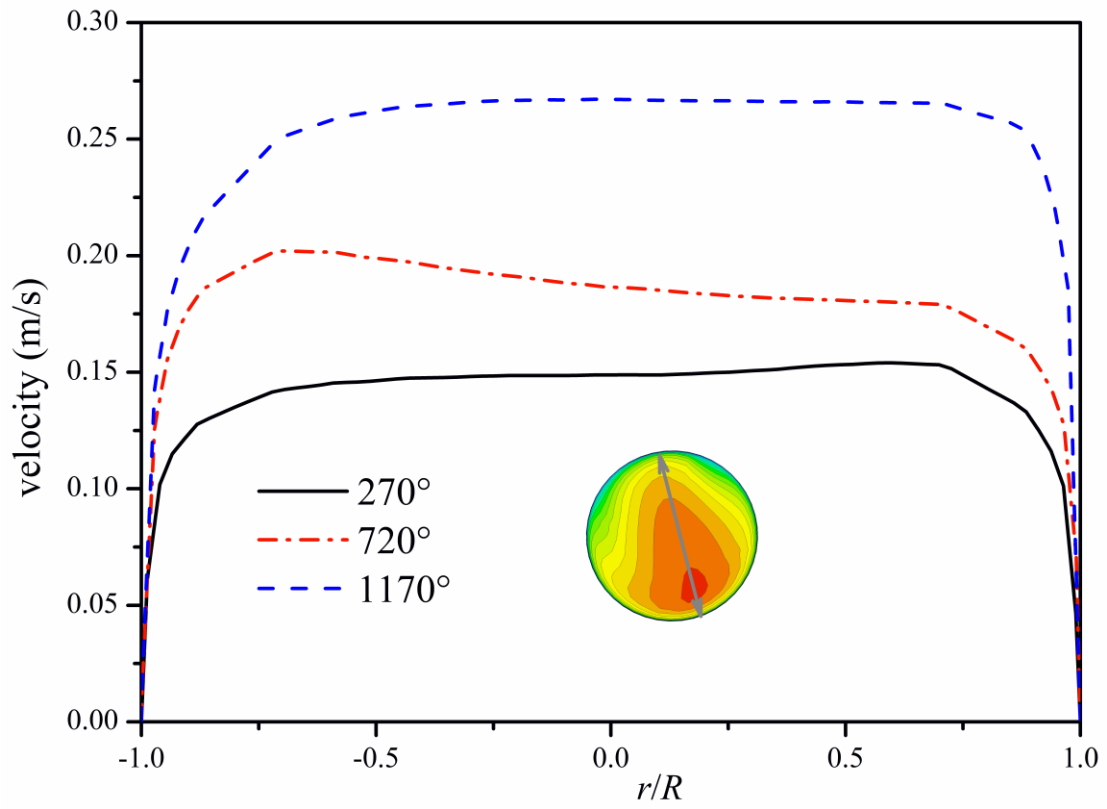
0.30
0.25
0.20
0.15
0.10
0.05
0.00
velocity (m/s)
-1.0
-0.5
0.0
0.5
1.0
r/R
270°
720°
1170°

Figure 9

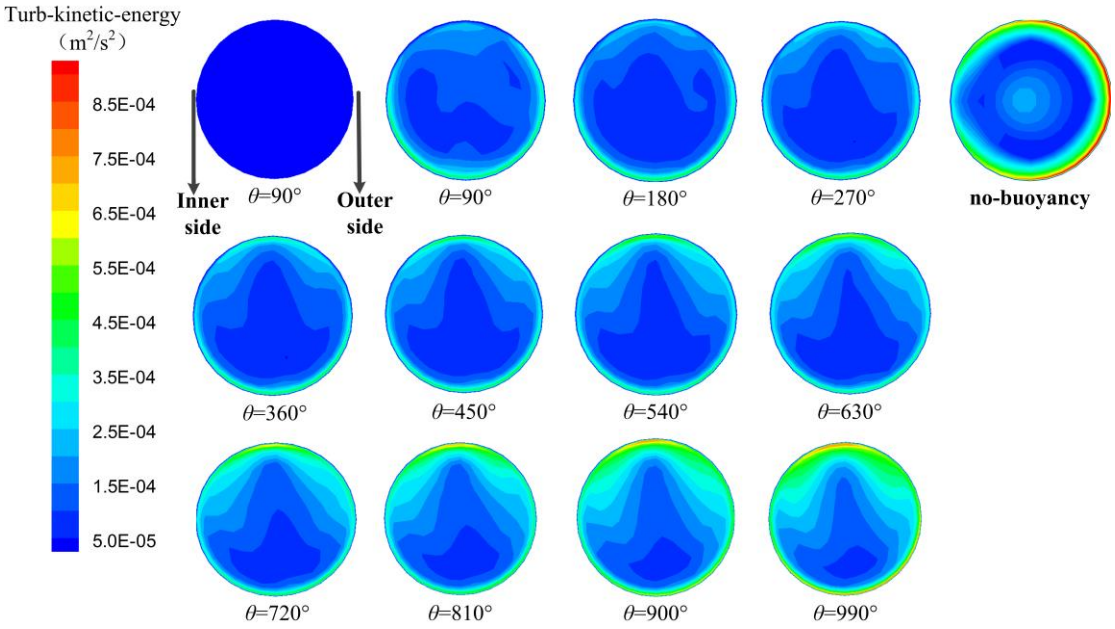
Turb-kinetic-energy
（m²/s²）
8.5E-04
7.5E-04
6.5E-04
5.5E-04
4.5E-04
3.5E-04
2.5E-04
1.5E-04
5.0E-05
Inner side
Outer side
θ=90°
θ=90°
θ=180°
θ=270°
no-buoyancy
θ=360°
θ=450°
θ=540°
θ=630°
θ=720°
θ=810°
θ=900°
θ=990°

Figure 10

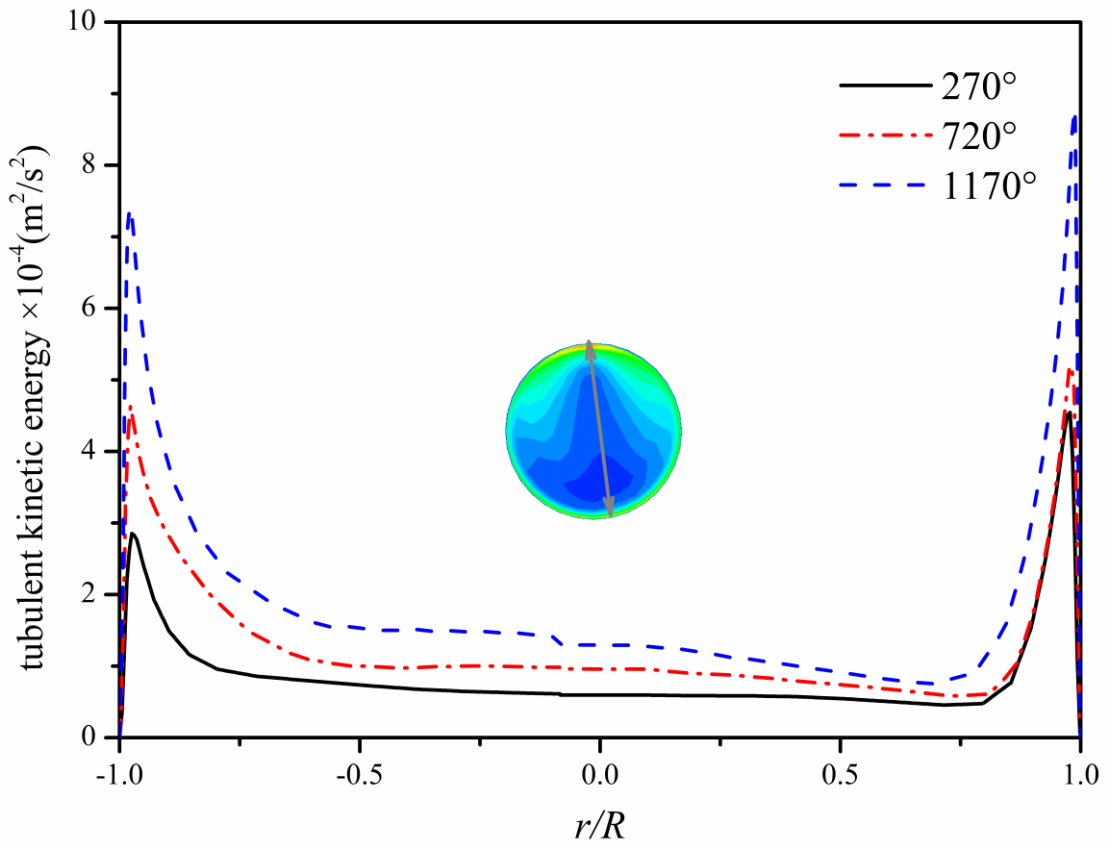
10
8
6
4
2
0
-1.0
-0.5
0.0
0.5
1.0
r/R
tubulent kinetic energy ×10-4(m2/s2)
270°
720°
1170°

Figure 11

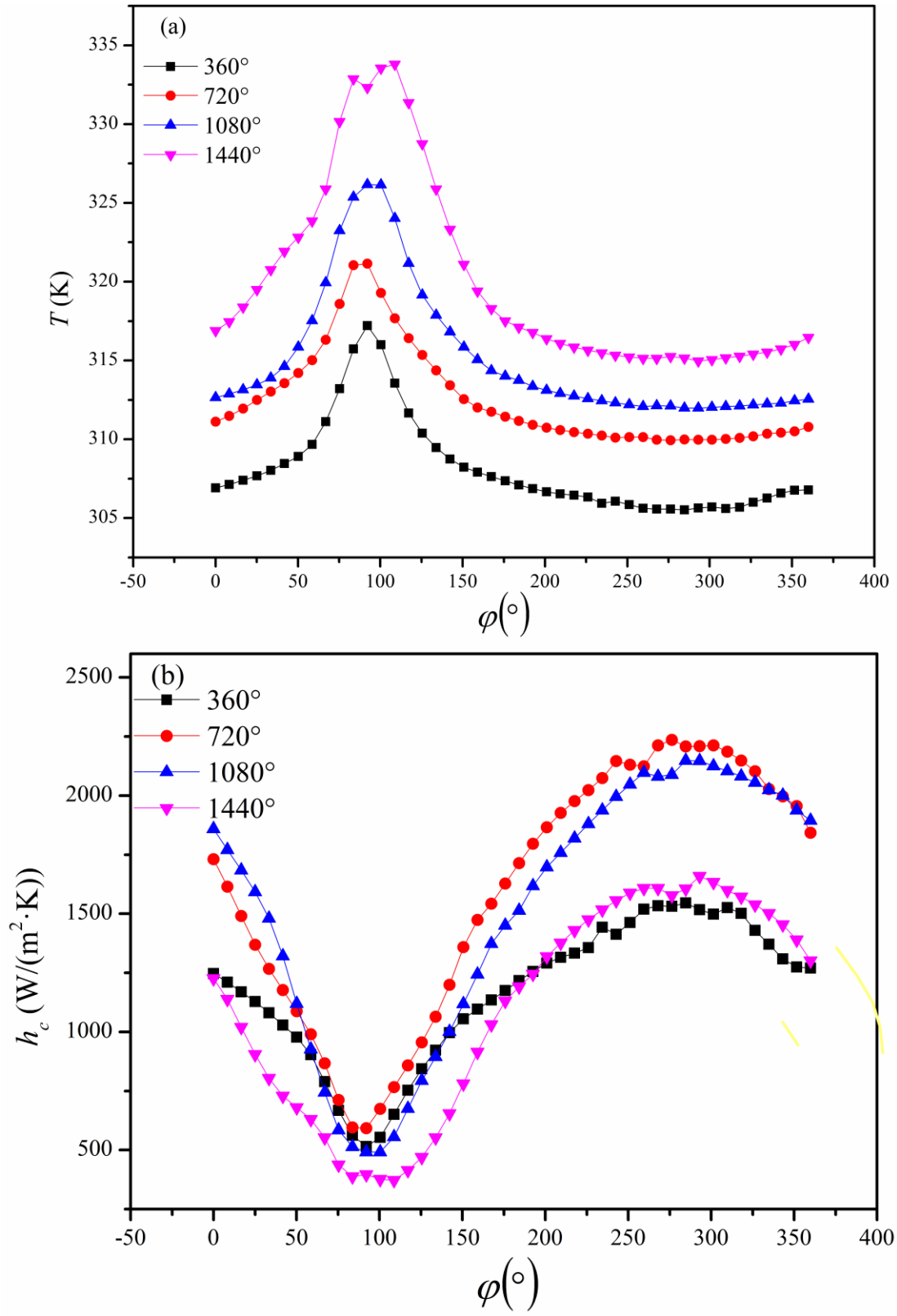
(a)
360°
720°
1080°
1440°
T (K)
335
330
325
320
315
310
305
-50
0
50
100
150
200
250
300
350
400
φ(°)
(b)
360°
720°
1080°
1440°
h_c (W/(m²·K))
2500
2000
1500
1000
500
-50
0
50
100
150
200
250
300
350
400
φ(°)

Figure 12

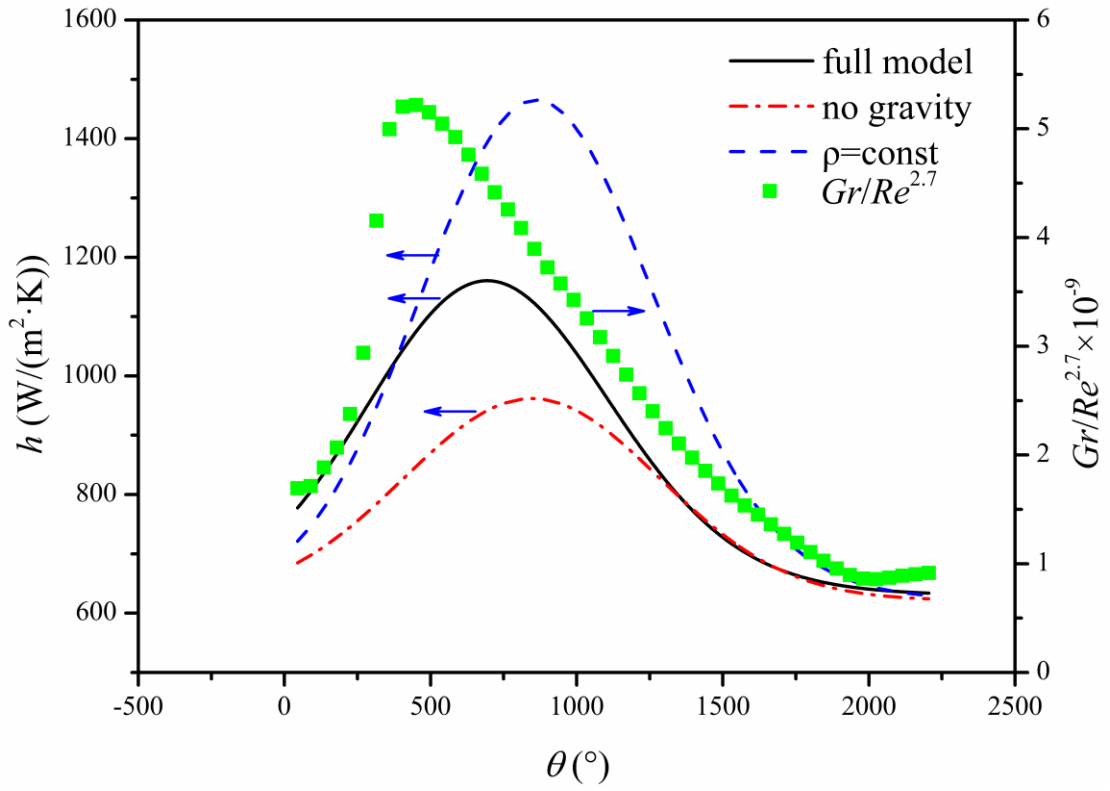
full model
no gravity
ρ=const
Gr/Re^2.7
h (W/(m^2·K))
Gr/Re^2.7×10^-9
θ(°)
1600
1400
1200
1000
800
600
6
5
4
3
2
1
0
-500
0
500
1000
1500
2000
2500

Figure 13

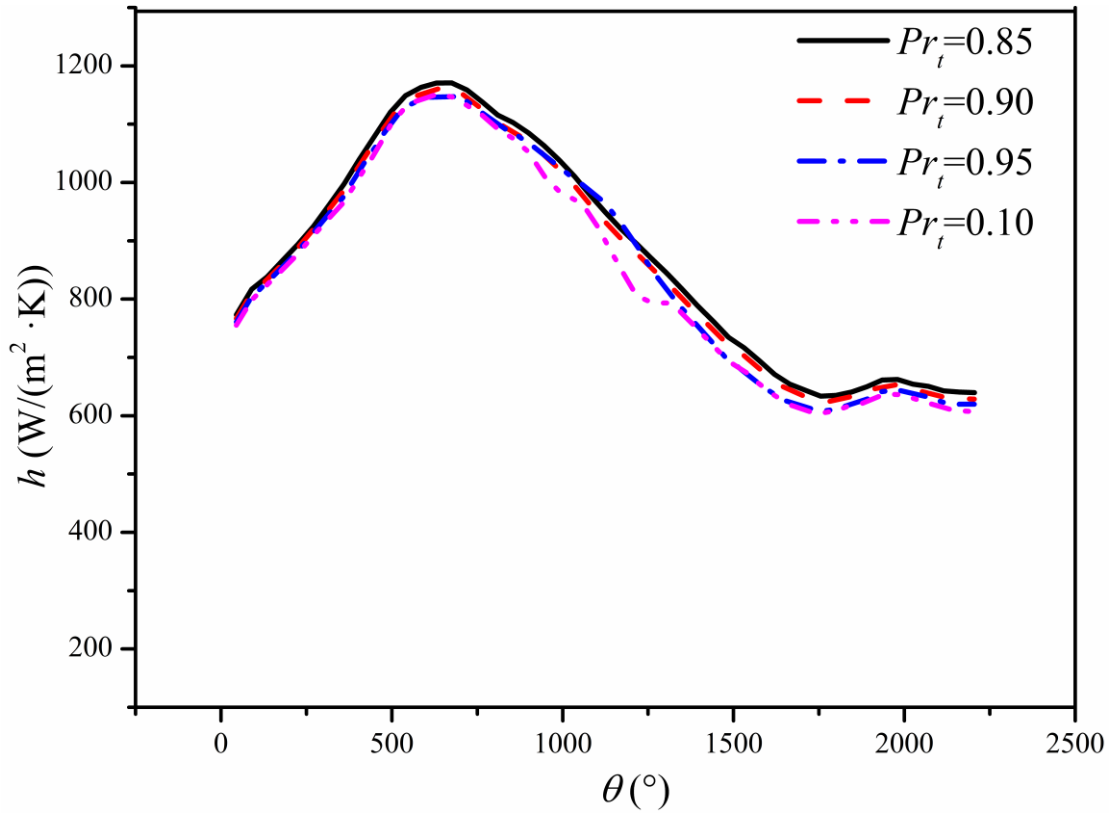
Pr_t=0.85
Pr_t=0.90
Pr_t=0.95
Pr_t=0.10
1200
1000
800
600
400
200
h (W/(m^2·K))
0
500
1000
1500
2000
2500
θ(°)

Table captions

Table 1 Detail of turbulence number models

(a) Constants used in the turbulence models , D and E terms

model	C_μ	$C_{\varepsilon 1}$	$C_{\varepsilon 2}$	σ_k	σ_ε	D	E
$k-\varepsilon$	0.09	1.44	1.92	1.0	1.3	0	0
RNG $k-\varepsilon$	0.085	$1.42-\frac{\eta(1-\eta/4.38)}{1+0.015\eta^3}$	1.68	0.7179	0.7179	0	0
SST	0.09	1.55	1.83	2.0	2.0	0	$-2\left(\nu+\frac{\nu_t}{2}\right)\frac{\partial k}{\partial y}\frac{\partial}{\partial y}(\frac{\varepsilon}{k})$
AB	0.09	1.45	1.83	1.0	1.4	0	0
LB	0.09	1.44	1.92	1.0	1.3	0	0
LS	0.09	1.44	1.92	1.0	1.3	$2\nu\left(\frac{\partial\sqrt{k}}{\partial y}\right)$	$2\nu\nu_t\left(\frac{\partial^2 u}{\partial y^2}\right)^2$
YS	0.09	1.44	1.92	1.0	1.3	0	$\nu\nu_t\left(\frac{\partial^2 u}{\partial y^2}\right)^2$
AKN	0.09	1.50	1.90	1.4	1.4	0	0
CHC	0.09	1.44	1.44	1.0	1.3	0	0

(b) Function used in the turbulence models

model	f_μ	f_1	f_2
$k-\varepsilon$	1.0	1.0	1.0
RNG $k-\varepsilon$	1.0	1.0	1.0
SST	1.0	1.0	1.0
AB	$\tanh\left(0.008\mathrm{Re}_y\right)\left(1+\frac{4}{\mathrm{Re}_t^{3/4}}\right)$	1.0	$1-\frac{2}{9}\exp\left(1-\frac{\mathrm{Re}_t^2}{36}\right)\times\left[1-\exp\left(\frac{-\mathrm{Re}_y}{12}\right)\right]$
LB	$\left[1-\exp\left(-0.0165\mathrm{Re}_y\right)\right]^2\times\left(1+\frac{20.5}{\mathrm{Re}_t}\right)$	1.0	$1-\exp\left(-\mathrm{Re}_t^2\right)$
LS	$\exp\left[\frac{-3.4}{\left(1+\mathrm{Re}_t/50\right)^2}\right]$	1.0	$1-0.3\exp\left(-\mathrm{Re}_t^2\right)$
YS	$\left(1+1/\sqrt{\mathrm{Re}_t}\right)\left[1-\exp\begin{pmatrix}-1.5\times10^{-4}\,\mathrm{Re}_y\\-5.0\times10^{-7}\,\mathrm{Re}_y^3\\-1.0\times10^{-10}\,\mathrm{Re}_y^5\end{pmatrix}\right]$	$\frac{\sqrt{\mathrm{Re}_t}}{1+\sqrt{\mathrm{Re}_t}}$	$\frac{\sqrt{\mathrm{Re}_t}}{1+\sqrt{\mathrm{Re}_t}}$
AKN	$\left\{1-\frac{5}{\mathrm{Re}_t^{0.75}}\exp\left[-\left(\frac{\mathrm{Re}_t}{200}\right)^2\right]\right\}\times\left[1-\exp\left(-\frac{y^*}{14}\right)\right]^2$	1.0	$\left\{1-0.3\exp\left[-\left(\frac{\mathrm{Re}_t}{6.5}\right)^2\right]\right\}\times\left[1-\exp\left(-\frac{y^*}{3.1}\right)\right]^2$
CHC	$\left[1-\exp\left(-0.0215\mathrm{Re}_y\right)\right]^2\times\left(1+\frac{31.66}{\mathrm{Re}_t^{5/4}}\right)$	1.0	$\left[1-0.01\exp\left(-\mathrm{Re}_t^2\right)\right]\times\left[1-\exp\left(-0.0631\mathrm{Re}_y\right)\right]$
Note:	$\eta=Sk/\varepsilon$, $S=\left(2S_{ij}S_{ij}\right)^{0.5}$, $S_{ij}=\frac{1}{2}\left(\frac{\partial u_i}{\partial x_j}+\frac{\partial u_j}{\partial x_i}\right)$, $\mathrm{Re}_t=\frac{k^2}{\nu\varepsilon}$, $\mathrm{Re}_y=\frac{yk^{0.5}}{\nu}$, $y^*=\frac{y}{\nu}u_\varepsilon$, $u_\varepsilon=\left(\nu\varepsilon\right)^{0.25}$		

Table 2 The check of mesh independency

Cases	Number of cells	The average relative error
Case-1	1969418	0.216 %
Case-2	2402356	0.0769%
Case-3	3596970	0%

Table 3 Selected numerical investigations on heat transfer of supercritical fluids

Reference	Supercritical fluid	Turbulence models	The best model
Dang, *et al*. [18]	CO_2	JL model, LS model, MK model	LS model
He, *et al*. [40]	CO_2	LS model, CH model, LB model, AKN model, WI model, MK model, YS model, V2F model	V2F model
Jiang, *et al*. [12]	CO_2	RNG $k-\varepsilon$ model, YS model, AKN model, LB model	YS model
Yang, *et al*. [41]	CO_2	LB model, YS model, AKN model, RNG $k-\varepsilon$ model	LB model
He, *et al*. [42]	CO_2	LS model	LS model
He, *et al*. [21]	CO_2	AKN model, V2F model	AKN model
Jaromin, *et al*. [43]	H_2O	SST model	SST model

Note: the best model is defined that the model gives the best prediction to the experimental data